

## Article

# Fabrication of Novel Agrowaste (Banana and Potato Peels)-Based Biochar/TiO<sub>2</sub> Nanocomposite for Adsorption of Cr(VI), Statistical Optimization via RSM Approach

Aamna Ashfaq<sup>1,2</sup>, Raziya Nadeem<sup>2,\*</sup>, Hongyu Gong<sup>1</sup>, Umer Rashid<sup>3,\*</sup> , Saima Noreen<sup>2</sup>, Shafique ur Rehman<sup>2</sup>, Zubair Ahmed<sup>2</sup>, Muhammad Adil<sup>2</sup>, Nayab Akhtar<sup>4</sup>, Muhammad Zeeshan Ashfaq<sup>1</sup>, Fahad A. Alharthi<sup>5</sup> and Elham Ahmed Kazerooni<sup>6</sup> 

- <sup>1</sup> Key Laboratory for Liquid-Solid Structural Evolution & Processing of Materials, Ministry of Education, School of Materials Science and Engineering, Shandong University, Jinan 250061, China; amnaashfaq9@yahoo.com (A.A.); hygong@email.sdu.edu.cn (H.G.); zee4194202@gmail.com (M.Z.A.)
- <sup>2</sup> Department of Chemistry, University of Agriculture, Faisalabad 38040, Pakistan; saima\_bashir03@yahoo.com (S.N.); shafiq.urrehman@uaf.edu.pk (S.u.R.); 2015ag847@uaf.edu.pk (Z.A.); muhammadadil507@gmail.com (M.A.)
- <sup>3</sup> Institute of Nanoscience and Nanotechnology (ION2), Universiti Putra Malaysia, Serdang 43400, Selangor, Malaysia
- <sup>4</sup> Department of Zoology, Lahore College for Women University, Lahore 54000, Pakistan; nayabzeeshan7863@gmail.com
- <sup>5</sup> Chemistry Department, College of Science, King Saud University, Riyadh 1145, Saudi Arabia; fharthi@ksu.edu.sa
- <sup>6</sup> Department of Applied Biosciences, Kyungpook National University, Daegu 41566, Korea; elham.ghasemi.k@gmail.com
- \* Correspondence: raziyaanalyst@uaf.edu.pk (R.N.); umer.rashid@upm.edu.my or dr.umer.rashid@gmail.com (U.R.); Tel.: +603-97697393 (U.R.)



**Citation:** Ashfaq, A.; Nadeem, R.; Gong, H.; Rashid, U.; Noreen, S.; Rehman, S.u.; Ahmed, Z.; Adil, M.; Akhtar, N.; Ashfaq, M.Z.; et al.

Fabrication of Novel Agrowaste (Banana and Potato Peels)-Based Biochar/TiO<sub>2</sub> Nanocomposite for Adsorption of Cr(VI), Statistical Optimization via RSM Approach. *Polymers* **2022**, *14*, 2644. <https://doi.org/10.3390/polym14132644>

Academic Editors: Xin Zhou, Wei Zhang, Peng Zhang, Bin Ji and Shujuan Meng

Received: 2 June 2022  
Accepted: 23 June 2022  
Published: 29 June 2022

**Publisher's Note:** MDPI stays neutral with regard to jurisdictional claims in published maps and institutional affiliations.



**Copyright:** © 2022 by the authors. Licensee MDPI, Basel, Switzerland. This article is an open access article distributed under the terms and conditions of the Creative Commons Attribution (CC BY) license (<https://creativecommons.org/licenses/by/4.0/>).

**Abstract:** In this research work, a simple, efficient, and eco-friendly procedure for the biosorption of Cr(VI) ions was studied. A detailed comparative study was performed to check the adsorption efficiency of agrowaste (banana and potato peels)-based adsorbents. Firstly, mixed biosorbent was washed, dried and ground into powder, secondly, biosorbent was pyrolyzed into biochar and thirdly TiO<sub>2</sub> nanocomposite (TiO<sub>2</sub> NC) biosorbent was made by sonicating using prepared biochar and TiO<sub>2</sub> NPs. Titanium dioxide nanoparticles (TiO<sub>2</sub> NPs) were synthesized by a green method using *Psidium guajava* leaf extract. The synthesized adsorbents were characterized by SEM, EDX FT-IR, XRD and UV-visible analysis. The effect of four different factors, i.e., pH of the synthetic metallic solution, time, concentration and adsorbent dosage was studied. The optimum conditions were time (120 min), pH (3), concentration (10 ppm) and adsorbent dosage (1.0 g). The kinetic modeling showed that the adsorption of Cr(VI) ion follows a pseudo second-order mechanism and the Langmuir isotherm model was found to fit better for this study. Response surface methodology (RSM)-based optimized parameters provided optimal parameter sets that better represent the adsorption rate models. The uptake capacity of Cr(VI) from aqueous solution was found to be biomass (76.49 mg/L) < biochar (86.51 mg/L) < TiO<sub>2</sub> NC (92.89 mg/L). It can be suggested that the produced TiO<sub>2</sub> NC could possibly be an efficient biosorbent for the removal of Cr(IV).

**Keywords:** TiO<sub>2</sub> nanocomposite (TiO<sub>2</sub> NC); biomass; biochar; green synthesis; kinetic model; equilibrium model

## 1. Introduction

The prime component that is responsible for life on earth is water. It should be pollutant-free for drinking and other domestic and industrial activities. Natural resources are being contaminated with the increase in population and industrialization. A large

amount of water from industries is released which leads to water pollution causing dangerous effects on plants, human and marine life. Effluents discharged from the industries include heavy metals, pharmaceutical drugs, dyes and other effluents which affect the water quality [1]. Heavy metals pollution in the aquatic environment is a big problem due to its presence, contamination in the food chain and adverse effects on ecological and human health [2]. Many physical and chemical methods are used to remove heavy metals from wastewater [3]. Ultrafiltration membrane, coagulation, reverse osmosis, ozonation and photocatalytic degradation are methods to treat wastewater [2,3]. However, they have some limitations, e.g., being costly, time-consuming and producing secondary by-products. Adsorption is an appropriate method which is an effective, environment-friendly and economic method for eliminating toxic heavy metal ions from wastewater effluents [4]. This method is easy to plan and apply and permits us to generate extremely good-quality treated waste material. The adsorbents may be activated carbons, fly ash, clay minerals, zeolites, industrial waste, agricultural waste, biomass and polymeric materials, etc. [5]. Chromium is a model pollutant in this study, it badly affects the aquatic system. The permissible limit for chromium recommended by the environmental protection agency is 50 µg/L [6]. Chromium affects the body organs, when it enters through the lungs it causes chronic bronchitis, irritation, rhinitis, pharyngitis, hyperemia and mucous nasal membrane ulcers. Skin exposure causes irritation or dermatitis due to allergy. Chromium also causes cancer in the respiratory tract, mainly lung, sinus and nasal cancer. Other mild effects include weakness, eye irritation, dizziness, erosion or discoloration of teeth [6].

Green synthesis of nanomaterials requires no need for high pressure and temperature, using nontoxic materials and low cost leads to environmentally friendly products. Plant extracts have been used as stabilizers, capping agents and reducing agents [5]. Nanoparticles (NPs) have appeared as an excellent choice for dealing with the global issue of water pollution. Recently, the synthesis of nanoparticles with precise morphologies and properties has gained a lot of interest. The large surface area and unique physical, chemical and optical properties make them good adsorbents for a wide range of pollutants [7]. TiO<sub>2</sub> NPs have high redox potential, low toxicity and adjustable optoelectronic properties. They have several applications such as antifogging mirrors, solar cells and self-cleaning antibacterial coatings [8,9]. TiO<sub>2</sub> NPs are one of the most important photocatalytic materials because they are a wide-bandgap semiconductor material (~3.2 eV) suitable only to absorb UV light and, hence, photogenerate charge carriers, electrons in the conduction band and holes in the valence band [10–12]. They are novel and active photocatalysts for wastewater treatment due to their high stability, low cost and high efficiency. Heterogeneous photocatalysis using TiO<sub>2</sub> NPs has been an interesting method in wastewater treatment due to its ability to degrade organic contaminants [13].

Potato (*Solanum tuberosum*) peels contain vitamins, starch, non-starch polysaccharide, protein, acid-soluble/insoluble lignin, lipids and ash. They are reported as adsorbents for the removal of several heavy metals in literature [14]. Banana (*Musa acuminata*) peels have an affinity for heavy metal adsorption because of various potential groups such as amino, alkoxy hydroxyl and carbonyl groups [15]. Peels of bananas were reported to be used as adsorbents for several heavy metals [16]. Dried and ground biomass is used in the present study, 1:1 of both banana peels and potato peels is used to prepare mixed biomass (MBM) [17].

Biochar is a material that contains an abundant amount of carbon, and it is gained from biomass, it is preferable because it is easily available, has a wide surface area, a large amount of functional groups present on the surface area, a possible conversion process and eco-friendly behavior [18]. Synthesis of functional biochar of enhanced surface characteristics has great attention and is also a great challenge for the development of the adsorption process. Two main factors that greatly affect the surface property of biochar are biomass type and its carbonization [19]. Nanocomposite is a matrix in which nanoparticles are loaded due to which surface area and stability is increased along with the properties of nanomaterials such as thermal conductivity, strength, surface area, etc. [20].

In the present research work, TiO<sub>2</sub> NPs were synthesized using *Psidium guava* leaf extract and TTIP, then these TiO<sub>2</sub> NPs were loaded on a matrix to prepare the nanocomposite. This work aims to compare adsorption capacity mg/g of mixed biomass (MBM) (grounded banana and potato peels), biochar (BC) of prepared biomass and TiO<sub>2</sub>/agrowaste-based biochar nanocomposite (TiO<sub>2</sub> NC), which were made by using *Psidium guajava* leaf extract for the synthesis of nanoparticles and biochar of MBM as a matrix. Different parameters such as contact time, pH, initial concentration and adsorbent dosage were studied. Furthermore, the kinetic data and equilibrium of biosorption were tested using isotherm models (Langmuir and Freundlich) and two kinetic models (pseudo first-order and pseudo second-order).

## 2. Materials and Methods

### 2.1. Materials and Chemicals

Titanium tetra hydroxide (TTIP), sodium hydroxide (NaOH), hydrochloric acid (HCl), potassium dichromate (K<sub>2</sub>Cr<sub>2</sub>O<sub>7</sub>), acetone and ethanol were purchased from Merck, Chemical Company, Hamburg, Germany. All chemicals involved in this study are analytical reagent grade, and solutions were all prepared with deionized water. All dilutions have been made in double-distilled water. Glassware was cleaned and rinsed with double-distilled water. They were dried in an electric oven at 50–55 °C.

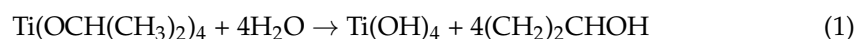
### 2.2. Preparation of Adsorbate Solution

A stock solution of hexavalent chromium Cr(VI) was prepared by dissolving 5.65 g of potassium dichromate (K<sub>2</sub>Cr<sub>2</sub>O<sub>7</sub>) in 1000 mL of distilled water. From the 1000 mg/L stock solution, 10 mL was diluted to 100 mL which gives a 100 mg/L (100 ppm) working solution. Experimental solutions of desired concentration were then obtained by successive dilutions. The initial pH measurements were performed by pH instrument and were calibrated using the buffer solutions of pH values. The pH of the synthetic contaminated water was modified by the addition of dilute NaOH and HCl solutions.

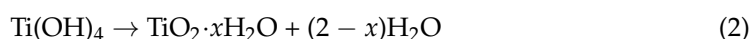
### 2.3. Synthesis of Biosorbents

In this work, three biosorbents were made for comparative study. Firstly, mixed biomass (MBM) was prepared by collecting peels of banana (*Musa acuminata*) and potato (*Solanum tuberosum*) from local market and household waste. They were washed properly and rinsed with deionized water to remove all dust particles and then dried in sunlight for a week. The dried peels of agrowaste (banana and potato peels) were ground into a fine powder with a pestle and mortar then it was passed through the sieve to get a particle size of ~0.5 mm. Then they were stored in hermetic plastic bags for further use [21]. Secondly, the MBM was pyrolyzed at 550 °C for 2 h at a heating rate of 2 °C min<sup>-1</sup>. The resulting biosorbent is biochar (BC) [22]. Lastly, to prepare TiO<sub>2</sub> NPs had been prepared by green synthesis method using Titanium Tetraisopropoxide (TTIP) and extract of guava leaves [23]. The plausible mechanism for synthesis of TiO<sub>2</sub> NPs could be following:

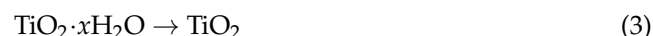
Hydrolysis:



Condensation:



Crystallisation via calcination:



where  $x$  = number of water molecules.

TiO<sub>2</sub> nanoparticles were formed when TTIP undergo hydrolysis and condensation. Initially, When TTIP undergoes hydrolysis, (Ti(OH)<sub>4</sub>) was formed as an intermediate as

shown in Equation (1).  $\text{Ti}(\text{OH})_4$  undergoes condensation as it is usually not stable and amorphous hydrous oxide precipitates ( $\text{TiO}_2 \cdot x\text{H}_2\text{O}$ ) were formed as stated in Equation (2). The formed  $\text{TiO}_2 \cdot x\text{H}_2\text{O}$  precipitates were then subjected to the calcination process at  $500^\circ\text{C}$  to remove the water molecules to form the crystalline  $\text{TiO}_2$  NPs as in Equation (3) [24].

#### 2.4. Characterization of Biosorbents

The prepared adsorbents were characterized by different analytical techniques, the elemental composition was studied through EDX. The prepared  $\text{TiO}_2$  NPs were confirmed through the UV-visible spectrophotometer (UV-2250, Shimadzu, Tokyo, Japan). Then, 50 mg of BC was sonicated with ethanol and then  $\text{TiO}_2$  NPs were added to dispersed BC. The developed dispersed mixture was ultrasonicated for 3 h followed by drying at moderate conditions to remove the solvent. After drying, the prepared nanocomposite was deposited on a petri dish and subjected to microwave irradiation for 2 min to give better exfoliation [25]. XRD technique (BTX III Benchtop XRD Analyzer, Olympus Corporation, Tokyo, Japan) was used to find if adsorbents had crystalline structure. Particle size was calculated through Scherrer's formula, which is given as:

$$D = K \frac{\lambda}{\beta \cos \theta} \quad (4)$$

where,  $K$  is a constant,  $\lambda$  is the wavelength of radiation and  $\beta$  is the full width half maximum.

Functional groups were determined through FT-IR (Perkin Elmer FT-IR Spectrophotometer, Waltham, MA, USA). The surface morphology of biosorbents before and after the experiment was studied by SEM (Carl Zeiss AG-SUPRA 35 VP SEM, Oberkochen, Germany).

#### 2.5. Optimization of Process Parameters Methodology

A batch adsorption experiment was conducted to optimize the parameters. The removal efficiency of Cr(IV) was examined by different parameters. All glassware and apparatus were washed with nitric acid and then with distilled water for removing impurities and dust particles. In this way, all types of Cr (VI) contamination were removed from the apparatus, and it was ready for further use under experimental conditions. For investigating of adsorption behavior of Cr(VI), pH values were optimized (1, 3, 5, 7, 10), as was the metal initial concentration range (10, 20, 40, 60, 80, 100 ppm). Contact time was also optimized at (30, 60, 120, 180, and 240 min). For maintaining the pH of the solution, 1M sodium hydroxide (NaOH) and hydrochloric acid (HCl) was used. After all these steps, experimental flasks were removed from the orbital shaker. The filter paper was used to filter the suspensions of nanocomposite and biomass and primary tests were performed to find out the equilibrium time. The concentration of residual Cr(VI) in samples was determined by atomic absorbance spectrophotometer. The amount of Cr(IV) removal was calculated using the following formula:

$$q = \frac{(C_i - C_e)v}{C_i} x \quad (5)$$

where  $C_i$  and  $C_e$  are the Cr (IV) concentrations in mg/L initially and at a given time,  $v$  is the volume of solution (L) and  $m$  is the mass of the adsorbent (g).

The potential rate-controlling step and kinetic mechanism of Cr(VI) biosorption were evaluated by adsorption kinetic. The equation of the pseudo 1st-order regression model for adsorption is stated as follows:

$$\log(qe) - \left( k \frac{1}{0.2303} \right) t \quad (6)$$

where,  $qe$  = amount of Cr(VI), and  $q$  (mg/g) = amount of Cr(VI) that is adsorbed on the adsorbents at equilibrium state,  $t$  is the time to achieve the equilibrium, the unit used for

these amounts is mg/g,  $k_1$  ( $\text{min}^{-1}$ ) represents the rate constant for the pseudo 1st-order reaction equation. Data of adsorption kinetics was again studied by pseudo 2nd-order kinetic model which presumes that sorption rate depends on adsorption capacity. The square of unoccupied sites is proportional to the sorption rate. It is shown as

$$\frac{t}{q} = \frac{1}{k_2 q_e^2} + \frac{t}{q_e} \quad (7)$$

where,  $k_2$  = equilibrium rate constant (g/mg/min). The slopes and intercept of plots  $t/q$  versus  $t$  were used to calculate the pseudo 2nd order rate constant  $k_2$  and  $q_e$ .

Equilibrium modeling was used to define the relationship between adsorbent and adsorbate molecules in an aqueous solution. The Langmuir isotherm equation is written as

$$\frac{C_i}{q_e} = \frac{1}{q_{max}} + \frac{1}{b q_{max}} C_e \quad (8)$$

where,  $C_e$  = equilibrium concentration,  $q_e$  = equilibrium adsorption capacity,  $b$  = slope and  $1/q_{max}$  = Intercept obtained from regression equation. The linear equation of Langmuir isotherm is written as

$$\frac{C_e}{q_e} = \frac{1}{X_m} KL + \frac{C_e}{X_m} \quad (9)$$

where,  $C_e$  = equilibrium concentration,  $q_e$  = amount of lead adsorbed at equilibrium,  $X_m$  and  $KL$  are Langmuir constants obtained by using the linearized Langmuir equation and Langmuir parameters.

The Freundlich isotherm equation is generally written as

$$q_e = K C_e \frac{1}{n} \quad (10)$$

The linear equation for the Freundlich isotherm is

$$\text{Log } q_e = \text{log } Kf + \left(\frac{1}{n}\right) \text{log } C_e \quad (11)$$

where,  $q_e$  (mg/g) = quantity of Cr (VI) adsorbed by specified amount of adsorbent at equilibrium,  $C_e$  (mg/L) = equilibrium concentration,  $Kf$  = intercept constant obtained from regression equation, and  $1/n$  = slope constant obtained from regression equation [26].

The interaction and optimization of three important independent variables, i.e., pH, initial concentration of Cr(VI) and adsorbent dosage were investigated by using response surface methodology. The Box–Behnken design was applied to predict and model the complex relations between the 3 parameters (pH, concentration and adsorbent dosage). The polynomial model was calculated through Design Expert 8.0 software and the formula could be described by Equation (12):

$$R(\%) = a_0 + \sum_{i=1}^n a_i X_i + \sum_{i=1}^n a_{ii} X_i^2 + \varepsilon \quad (12)$$

where  $a$  was the coefficient;  $X$  was the independent variable, and  $\varepsilon$  was the random error [27].

### 3. Results and Discussion

#### 3.1. Characterization of Adsorbent

##### 3.1.1. UV Analysis of TiO<sub>2</sub> NPs

Synthesis was confirmed by a UV/visible spectroscopy peak of maximum absorption observed between 290 and 310 nm. These results confirmed the synthesis of TiO<sub>2</sub> NPs. A maximum absorption peak was observed at 295 nm, the UV spectrum is shown in Figure 1.

The results agreed with previously reported literature, where the peak was observed at 310 nm [28,29].

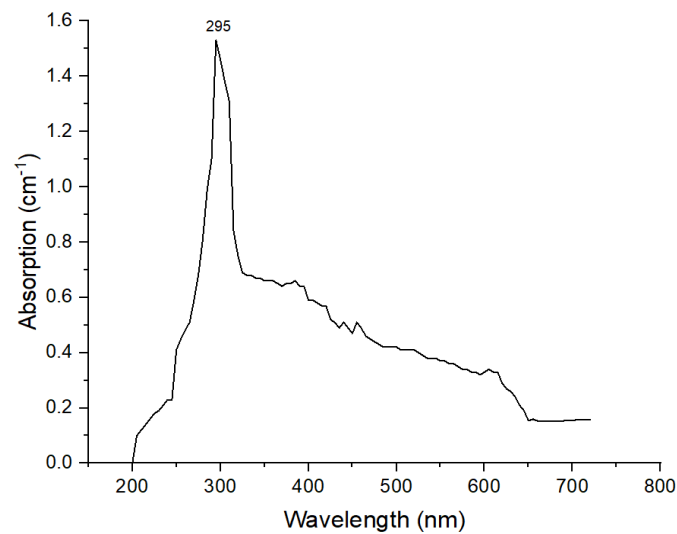


**Figure 1.** UV spectra of TiO<sub>2</sub> NPs.

### 3.1.2. Scanning Electron Microscopy (SEM) and EDX Analysis

The morphology of prepared adsorbents is described in Figure 2. SEM micrographs of the MBM, BC and TiO<sub>2</sub> NC are shown in Figure 2a–c which shows the bulky and smooth morphology of the bare biosorbents. MBM has hollow spaces, while biochar and TiO<sub>2</sub> NC have agglomerated structures, Figure 2d–f shows Cr(VI) loaded biosorbents. A clear difference can be seen between the surface morphology of Cr(VI) loaded and unloaded biosorbents at the same magnification.

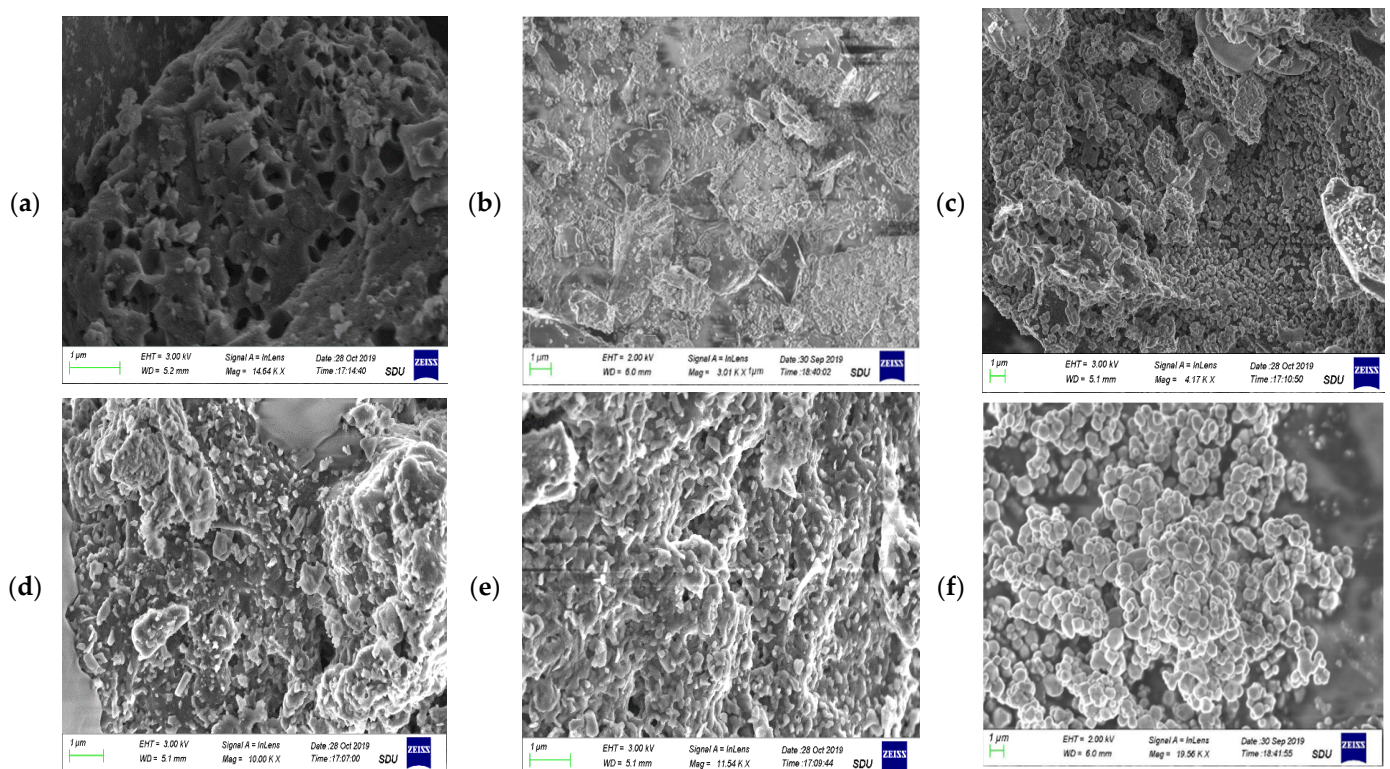


**Figure 2.** SEM micrograph of (a) biomass; (b) biochar; (c) TiO<sub>2</sub> NC; (d) lead-loaded biomass; (e) lead-loaded biochar; and (f) lead-loaded TiO<sub>2</sub> NC.

The elemental composition of prepared biosorbents was analyzed by EDX analysis. The higher the number of a particular element, the higher its presence in that point or area of interest. The EDX spectrum of TiO<sub>2</sub> NP is shown in Figure 3a. It is indicating strong Ti peaks at 0.7, 4.6 and 4.9 keV (1.2 cps/ev). The peak for oxygen also appeared at 0.5 keV (4.1 cps/ev). Figure 3b represents the elemental composition of MBM. Zr, Ca and O can be seen from the spectra. Figure 3c shows the spectra of TiO<sub>2</sub> NC. Table 1 shows the weight (%) and atomic (%) of the constituent elements of TiO<sub>2</sub> NP, MBM and TiO<sub>2</sub> NC.

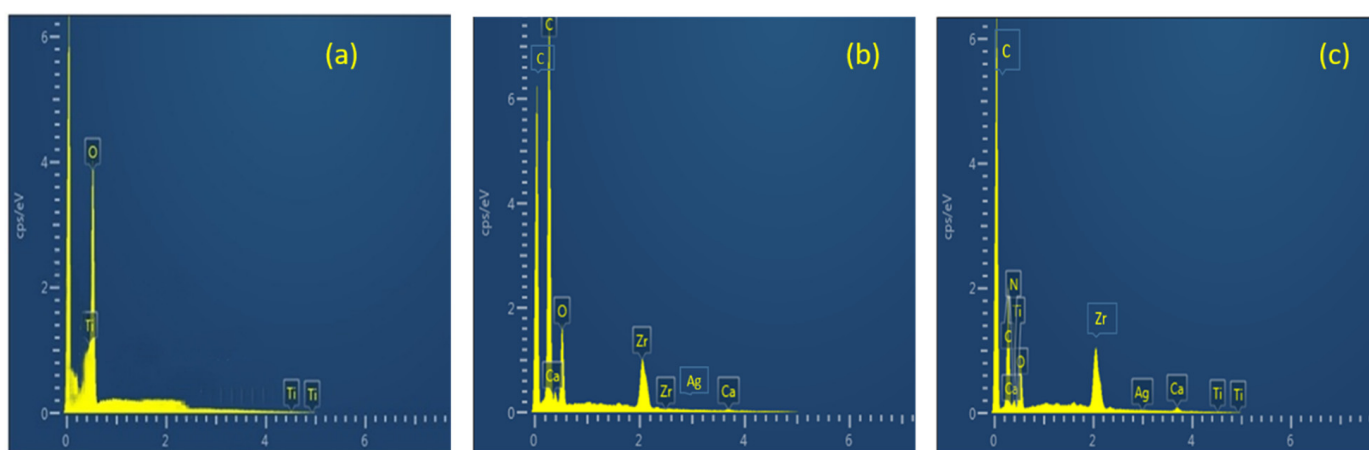


**Figure 3.** EDX spectra of (a) TiO<sub>2</sub> NP; (b) biomass; and (c) TiO<sub>2</sub> NC.

**Table 1.** Element composition of biomass, TiO<sub>2</sub> NP & TiO<sub>2</sub> NC.

Adsorbent	Elements Found	Weight %	Atomic %
Biomass	C	58.6	71.65
	Ca	24.68	10.71
	O	15.74	9.67
	Zr	0.08	3.51
	Ag	0.03	4.22
TiO <sub>2</sub> NP	Ti	70.5	68.43
	O	29.5	31.85
TiO <sub>2</sub> NC	Ti	41.69	74.84
	O	39.95	10.84
	Ca	9.65	7.54
	N	4.63	3.65
	C	3.1	2.91
	Zr	0.04	0.05
	Ag	0.61	0.09

### 3.1.3. FT-IR Spectroscopy

FT-IR is a nondestructive analytical technique used for identifying the chemical bonds in a matter with the interaction of infrared (IR) radiation. When the sample is exposed to IR light, some light is reflected but a large portion of IR light is absorbed (which causes the molecules to vibrate) by the sample. A molecular fingerprint of the sample is created by the transmitted light and the resulting spectrum represents absorption or transmission vs wavenumber. Every sample has a different composition and unique arrangement of atoms. FT-IR is helpful for the qualitative and quantitative analysis of organic and inorganic samples [30]. The molecular fingerprint of materials was examined through Fourier transform infrared spectroscopy, allowing close examination of a sample's chemical composition. FT-IR spectra of TiO<sub>2</sub> NP are shown in Figure 4a. From the spectra, no peaks are observed in the functional group because there is no functional group present in the prepared sample. The peaks are present at 498 cm<sup>-1</sup> to 550 cm<sup>-1</sup> these peaks are of O–Ti–O

and Ti–O bending vibrations. These peaks are present in the fingerprint region of the spectra. Broad peaks are present at  $1621.69\text{ cm}^{-1}$ , these peaks show the Ti–OH stretching vibration.

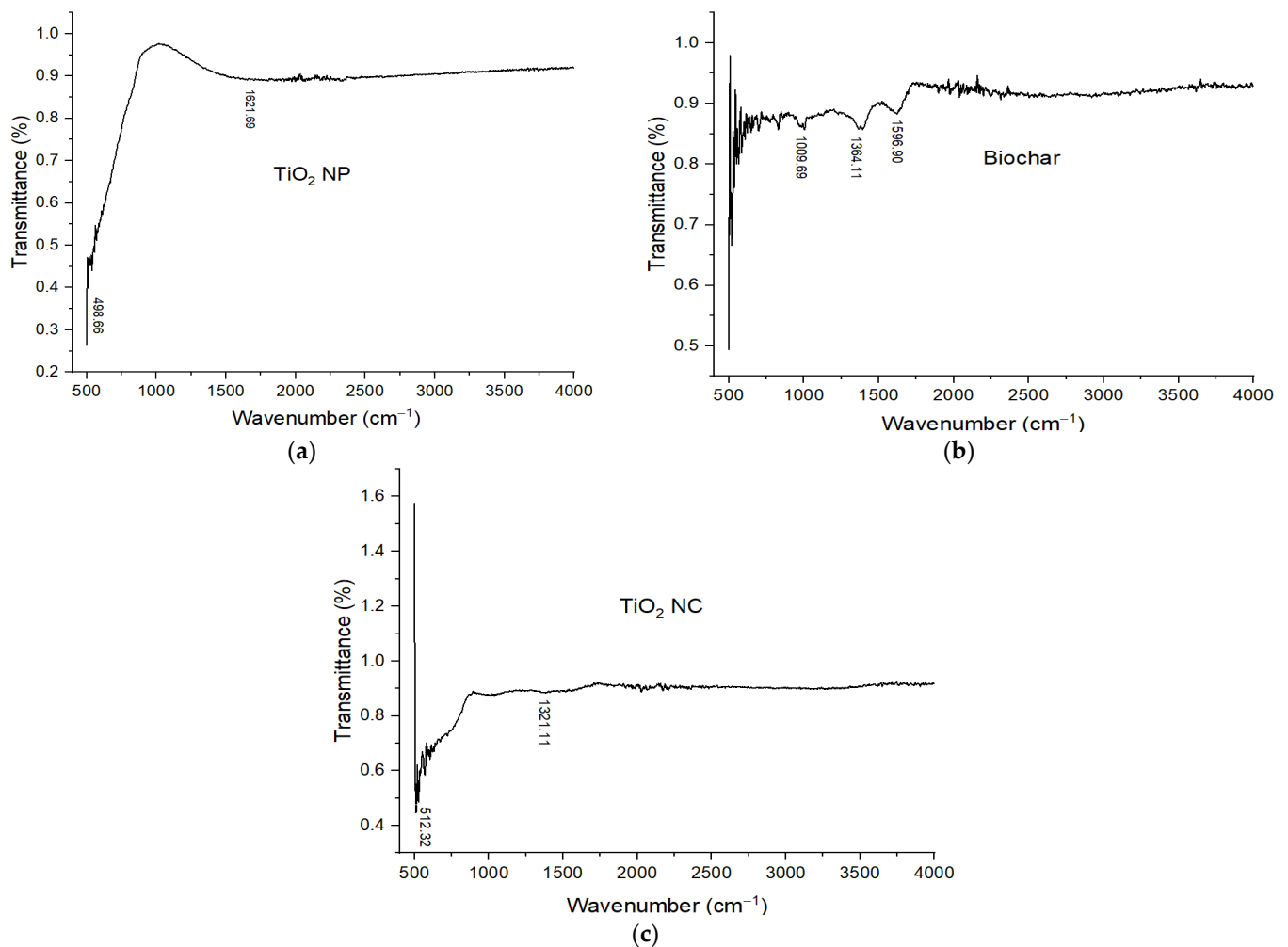


**Figure 4.** FT-IR spectra of (a)  $\text{TiO}_2$  NP; (b) biochar; and (c)  $\text{TiO}_2$  nanocomposite.

The FT-IR spectrum of BC is shown in Figure 4b. The absorption bands between  $1704\text{--}1612\text{ cm}^{-1}$  were assigned to C–O/C=O stretching vibrations of aromatic rings of lignin. A conjugated (Hibbert’s) ketone C=O band at  $1699\text{ cm}^{-1}$  might be derived from lignin demethylation of the aromatic methoxy group. Furthermore,  $2925\text{--}1375\text{ cm}^{-1}$  are the bending vibrations of  $\text{CH}_3$  and  $\text{CH}_2$ . So, the presence of abundant surface functional groups such as carboxyl and hydroxyl was confirmed which greatly enhanced the adsorption performance [28,29].

After combining biochar with  $\text{TiO}_2$  NPs, an increase in the relative peak intensity at about  $512.32\text{ cm}^{-1}$  is observed for  $\text{TiO}_2$  NC, which is often used for confirmation of vibration of Ti–O. Additionally,  $2925\text{--}1375\text{ cm}^{-1}$  are the bending vibrations of  $\text{CH}_3$  and  $\text{CH}_2$ . The FT-IR spectrum of  $\text{TiO}_2$  NC is shown in Figure 4c.

#### 3.1.4. XRD Diffraction Analysis of $\text{TiO}_2$ , MBM, BC and $\text{TiO}_2$ NC

In Figure 5a, strong diffraction peaks are present at  $2\theta$  values at  $25.19^\circ$ ,  $36.82^\circ$ ,  $37.65^\circ$ ,  $38.44^\circ$ ,  $47.92^\circ$ ,  $53.73^\circ$ ,  $54.93^\circ$  and  $61.96^\circ$  are associated with planes (011), (013), (004), (112), (020), (015), (121) and (024). These peaks are characteristic of  $\text{TiO}_2$ . The X-ray diffraction pattern at  $25.19^\circ$  and  $36.82^\circ$  indicates  $\text{TiO}_2$ , all peaks are under the standard spectrum (JCPDS No.: 88–1175 and 84–1286). This diffraction pattern shows that diffraction peak

intensity increases with increasing particle size [31], where the peaks of TiO<sub>2</sub> NP showed the anatase crystalline phase [32]. The average particle size of TiO<sub>2</sub> NP is found to be 11.73 nm. Lattice parameters are  $a = 3.78 \text{ \AA}$  and  $c = 9.53 \text{ \AA}$  and the system is tetragonal.

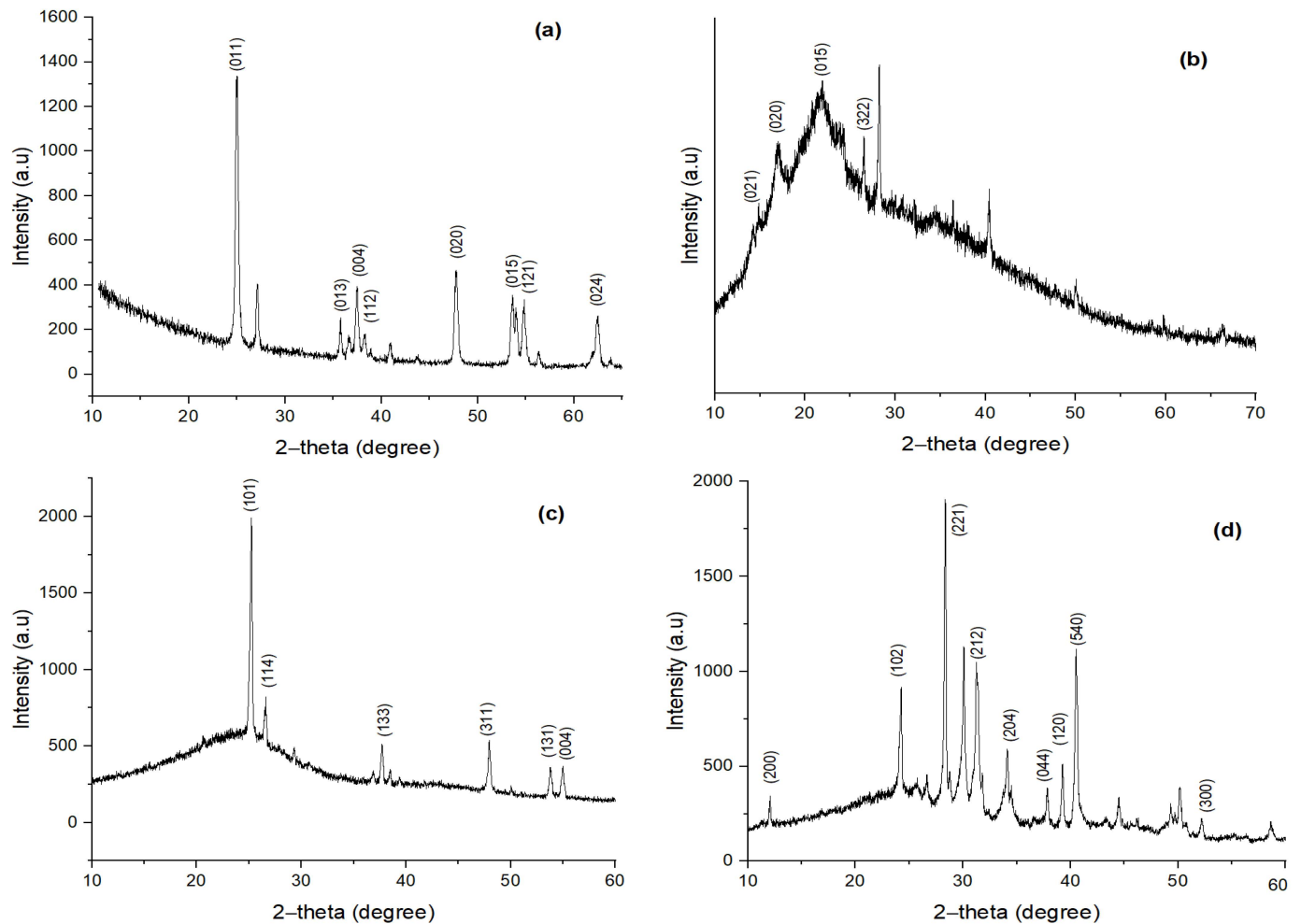


**Figure 5.** XRD pattern of (a) TiO<sub>2</sub> NP; (b) biomass; (c) biochar; and (d) TiO<sub>2</sub> NC.

Minor diffraction peaks showing a broad band represent the amorphous structure of MBM. These can be seen in Figure 5b. However, a couple of peaks can be seen at  $2\theta$  values. These are  $16.5^\circ$ ,  $23.6^\circ$ ,  $27.4^\circ$  and  $29.5^\circ$ , associated with planes (021), (020), (015) and (322). These are characteristic of a B-type crystalline structure [33,34]. The calculated particle size through Scherrer's formula was 0.013.

The diffraction pattern of BC is given in Figure 5c. Strong diffraction peaks are present at  $2\theta$  values at  $16^\circ$ ,  $19^\circ$ ,  $20.4^\circ$ ,  $24.6^\circ$ ,  $25.1^\circ$ ,  $27^\circ$ ,  $33.3^\circ$ ,  $38.2^\circ$  and  $42.2^\circ$  are associated with planes (021), (020), (051), (322), (202), (023), (230), (032) and (112). These signatures relate to crystalline carbon with expanded lattice parameters (carbon with impurities) [35]. The calculated particle size through Scherrer's formula was 0.932.

The diffraction pattern of TiO<sub>2</sub> NC is given in Figure 5d. Strong diffraction peaks are present at  $2\theta$  values at  $25.21^\circ$ ,  $26.63^\circ$ ,  $36.8^\circ$ ,  $47.74^\circ$ ,  $54.73^\circ$  and  $55.8^\circ$  are associated with planes (101), (114), (113), (311), (131) and (044). These strong peaks confirm the crystalline structure of novel TiO<sub>2</sub> NC. The calculated particle size through Scherrer's formula was 0.932.

### 3.2. Optimization of Process Parameters

#### 3.2.1. Effect of pH

The effect of pH on adsorption of Cr(VI) by biosorbents at different pHs ranging from 1 to 10 was observed to evaluate the optimum pH while other variables were kept constant, amount of adsorbent = 0.1 g, temp = 35 °C, shaking speed was 120 rpm and concentration was 100 ppm. In the solution, a decrease in removal efficiency occurs by increasing pH, and maximum removal was observed at 3. Removal efficiency decreases by increasing pH. It was investigated that the adsorbent revealed a comparable binding pattern for Cr(VI). The adsorbent surface becomes negatively charged. It is responsible for electrostatic interaction between adsorbent surface and metals that result in efficient removal of heavy metals. It was demonstrated that different adsorbents showed adsorption of Cr(VI) in comparison with each other. The maximum removal was observed at 92.89 mg/L for TiO<sub>2</sub> NC and maximum uptake in mg/L of Cr(VI) was decreased to 92.89 (TiO<sub>2</sub> NC) > 86.51 (BC) > 76.49 (MBM). The effect of pH on adsorption of Cr(VI) by using MBM, B and TiO<sub>2</sub> NC is graphically represented in Figure 6a.

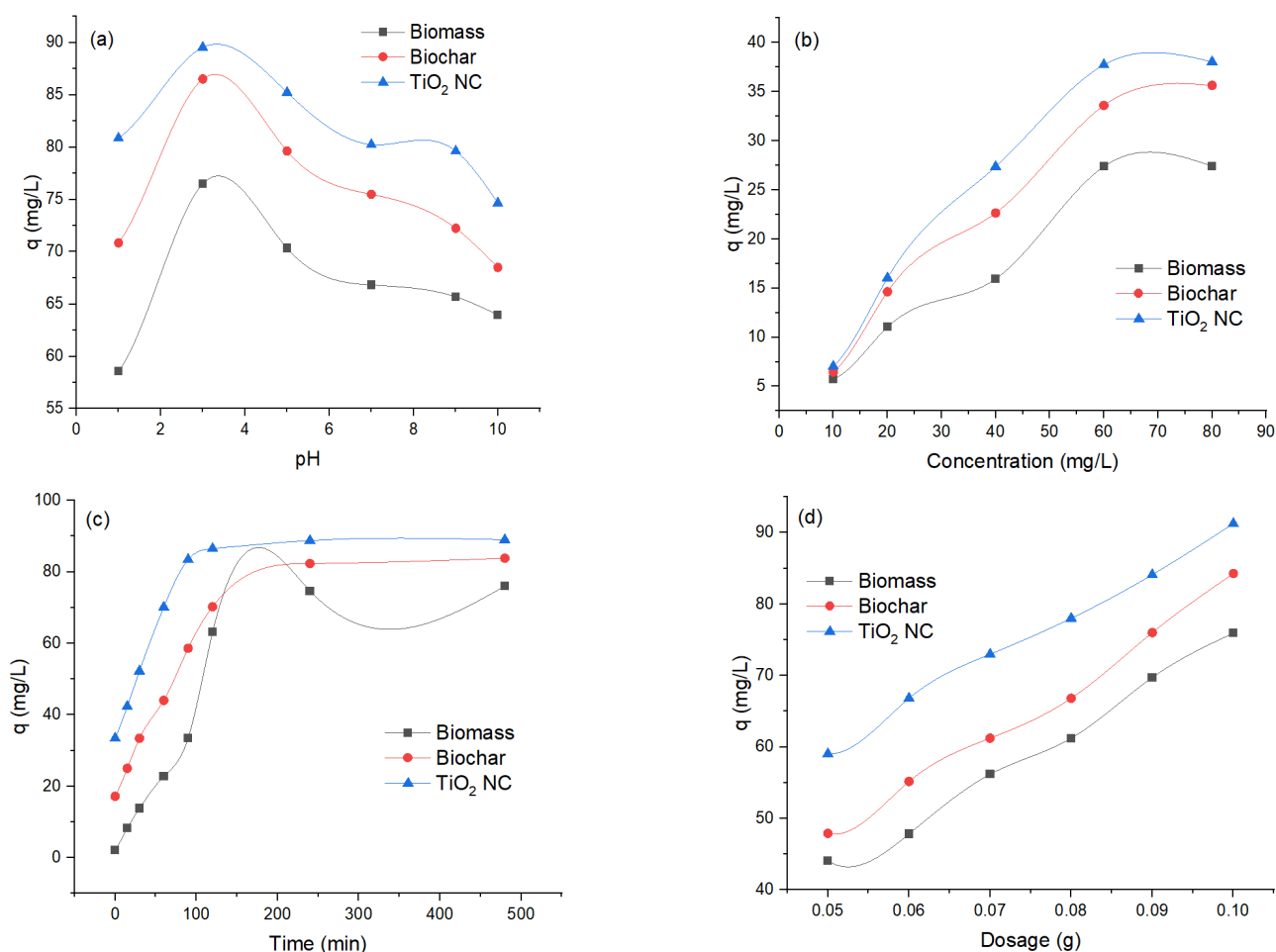


**Figure 6.** The effect of (a) pH; (b) concentration; (c) contact time; and (d) adsorbent dosage for removal of Cr(VI).

#### 3.2.2. Effect of Initial Concentration

Initial concentration is responsible for overcoming all barriers to the mass transfer of particles between the solid and liquid phases. The concentration of Cr(VI) solutions varied from 10 to 100 ppm. While other variables were kept constant, amount of adsorbent = 0.1 g, temp = 35 °C, shaking speed was 120 rpm and pH = 3. Results illustrated that percentage removal decreases with an increase in initial concentration. As the amount of adsorbent

is the same so competition was negligible at low concentrations but becomes prominent with the increase of concentration of adsorbate molecules. In simple words, the number of adsorption sites was limited at high solution concentrations which hinders the further uptake and hence the percentage removal decreases. The maximum removal was observed at 93.81 at 10 ppm for TiO<sub>2</sub> NC maximum uptake capacity in mg/L of Cr(VI) was decreased at 10 ppm as 93.81 (TiO<sub>2</sub> NC) > 86.34 (BC) > 76.64 (MBM). The effect of initial concentration on adsorption of Cr (VI) by using MBM, BC and TiO<sub>2</sub> NC is graphically represented in Figure 6b.

### 3.2.3. Effect of Contact Time

Contact time is a vital factor as it affects the process of adsorption. With the passage of time, more interaction occurs between adsorbent and adsorbate molecules due to which the adsorption rate is increased. In the present work, the effect of contact time on adsorption of Cr(VI) with different adsorbents were studied with a distinct time interval over a range from 15 to 120 min. While other variables were kept constant amount of adsorbent = 0.1 g, temp = 35 °C, shaking speed was 120 rpm, concentration = 100 ppm and pH = 3. The percentage removal efficiency increases as the time increases until equilibrium is achieved.

At the start of the process, there was a higher concentration gradient between adsorbent and heavy metals ions that sped up this process and percentage removal increased by increasing contact time from 0 to 120. At the initial stage of adsorption, a large number of vacant sites were available. As time passes, functional groups present on the surface of the adsorbent take part in the process of adsorption of heavy metals until equilibrium is achieved. The percentage removal increases with an increase in contact time and becomes constant after attaining equilibrium. After equilibrium, the adsorption process may get slow down due to the contribution of other processes, i.e., complexation, saturation of binding sites and micro-precipitation. As the equilibrium was achieved, no more Cr(VI) ions were further adsorbed by increasing contact time because there was no vacant site available resulting in optimization of contact time for the adsorption process. The maximum removal was observed at 88.97 for TiO<sub>2</sub> NC and maximum uptake in mg/L of chromium was decreased to 88.97 (TiO<sub>2</sub> NC) > 83.82 (BC) > 75.99 (MBM). The effect of contact time on adsorption of Cr(VI) by using MBM, BC and TiO<sub>2</sub> NC is graphically represented in Figure 6c.

### 3.2.4. Effect of Adsorbent Dosage

Cr(VI) removal efficiency as a function of adsorbents dosage was studied. The dose of the adsorbents varied between 0.05 g and 0.1 g, other studied parameters (pH, initial ion concentration and contact time) were kept optimum while temperature and agitation speed were kept at 25 °C and 200 rpm, respectively. Experiments have shown that increasing the dose of the adsorbents increased chromium removal efficiency. This is expected because more binding sites for ions are available at higher doses of adsorbents. These observations described that Cr(VI) adsorption in the wastewater is related to carbon surface area. The adsorbents with the highest surface area are more efficient for removing Cr(VI). The maximum uptake in mg/L of Cr(VI) was decreased to 91.27 (TiO<sub>2</sub> NC) > 84.27 (BC) > 75.93 (MBM). The effect of adsorbent dosage on adsorption of Cr (VI) by using MBM, BC and TiO<sub>2</sub> NC is graphically represented in Figure 6d.

### 3.2.5. Comparison among Different Adsorbents

The efficiency of all three adsorbents to remove Cr(VI) from liquid solution was shown in order TiO<sub>2</sub> NC > BC > MBM. The removal efficiency of TiO<sub>2</sub>NC was found to be highest and respectively followed by BC and MBM. The comparison of uptake capacity of three adsorbents is shown in Figure 7.

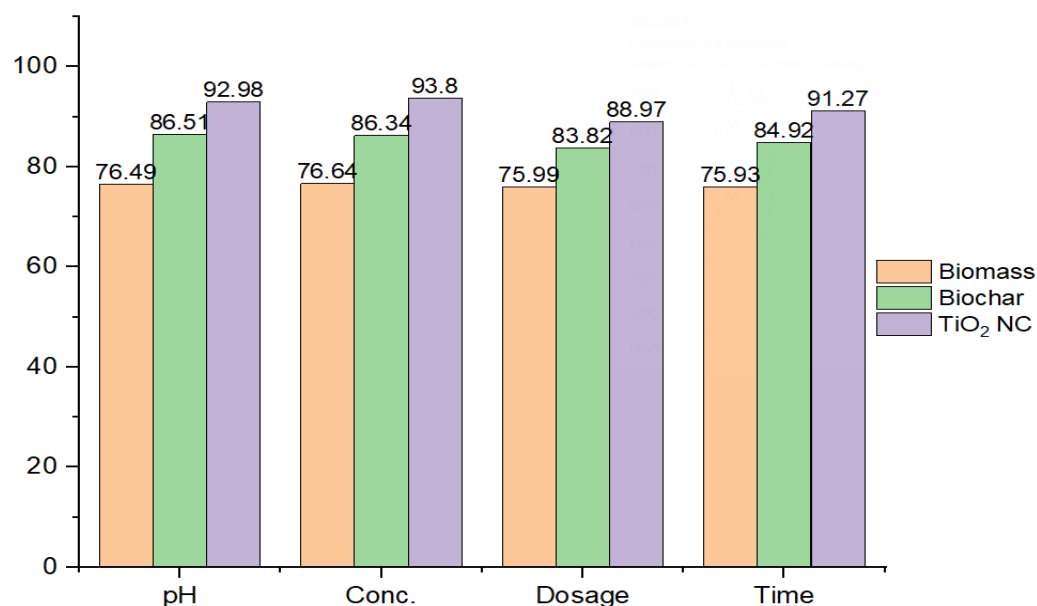


**Figure 7.** Comparison of adsorption efficiency by prepared adsorbents.

Q max results obtained in this work and compared with others reported in the literature, for the same adsorbate, are represented in Table 2.

**Table 2.** Comparison of adsorption efficiency of different adsorbents.

Adsorbate	Adsorbent	Q Max (mg/L)	References
Cr(VI)	Fe <sub>3</sub> O <sub>4</sub> /pinecones gel beads nanocomposite	212.22	[36]
	MoS <sub>2</sub> @LDC	198.70	[37]
	OB/ZnO	460.31	[38]
	Polymer-magnetic-algae nanocomposite	144.93	[39]
	Chitosan grafted graphene oxide (CS-GO) nanocomposite	104.16	[40]
Cr(VI)	Mixed biomass (banana and potato peels)	76.49	Present study
	Biochar	86.51	Present study
	TiO <sub>2</sub> /biochar nanocomposite	92.89	Present study

### 3.3. Adsorption Kinetics

To evaluate the potential rate-controlling step and kinetic mechanism of Cr(VI) biosorption on MBM, BC and TiO<sub>2</sub> NC pseudo first-order equation of Laguerre, pseudo second-order equation of Ho et al. [41]. Pseudo-1 nature because it only depends on several adsorbate molecules present in an aqueous solution at a definite time. However, the pseudo 2nd-order model describes that lead ions are present in an aqueous solution as well as many free active sites present on the surface of the adsorbent.

#### 3.3.1. Pseudo 1st-Order Model

The pseudo 1st-order regression model presumes that the rate of adsorption and unoccupied sites of Cr(VI) are proportional to each other. The intercept and slopes of the plot of the graph between the values of  $\log(q_e - q)$  time (t) were used for the calculation of pseudo 1st rate constant  $k_1$  and the capacity for the equilibrium adsorption. On comparison between pseudo 1st-order and pseudo 2nd-order reactions, it was found that the value of  $R^2$  in the case of 1st-order is less than that of 2nd-order, so the pseudo 1st-order model was not well fitted. Relatively lower  $R^2$  values were obtained for the pseudo 1st-order model,  $R^2$  values for Cr(VI) were MBM (0.70) > BC (0.78) and for TiO<sub>2</sub> NC (0.68). The theoretically calculated  $q_e$ (mg/g) did not agree well with experimentally calculated  $q_{exp}$ . The value of

correlation coefficients is lower than 1, most often equal to 0.8. This proves that it is not precise to use this model to conclude the adsorption kinetics by adsorbents MBM, BC and TiO<sub>2</sub> nanocomposite.

### 3.3.2. Pseudo 2nd-Order Model

Comparison between pseudo 1st-order, pseudo 2nd-order models, and kinetic parameters reveals that adsorption on the MBM, BC and TiO<sub>2</sub> NC are better fitted in pseudo 2nd-order kinetics than pseudo 1st-order, considering the q<sub>e</sub> value obtained from pseudo 2nd-order model. It was close to conformation with a value of experimental data value. While the value of q<sub>e</sub> evaluated from contrasting kinetic models did not comply with the experimental value. This shows that pseudo 1st-order is not satisfactory to explain the mechanism of Cr(VI) biosorption. Evaluation of kinetic data shows that R<sup>2</sup> values for the pseudo 1st-order and pseudo 2nd-order models are high >0.96 but q<sup>cal</sup> does not match with q<sup>exp</sup> to much extent [42]. A comparison of the values obtained from pseudo first-order and pseudo second-order models is given in Table 3 and their graphical representation is in Figure 8a,b.

Table 3. Comparison of pseudo 1st-order and 2nd-order.

Adsorbate	Adsorbent	Pseudo First-Order			Pseudo Second-Order			
		Q <sub>e</sub> (mg/g)	k <sub>1ad</sub> (min <sup>-1</sup> )	R <sup>2</sup>	Q <sub>exp</sub> (mg/g)	q <sub>e</sub> (mg/g)	k <sub>2ad</sub> (min <sup>-1</sup> )	R <sup>2</sup>
Chromium	Biomass	39.64	−0.0012	0.707	51.67	47.61	0.00048	0.891
	Biochar	45.04	−0.0036	0.789	68.23	85.47	0.00037	0.946
	TiO <sub>2</sub> NC	23.80	−0.0034	0.684	76.75	94.33	0.00074	0.991

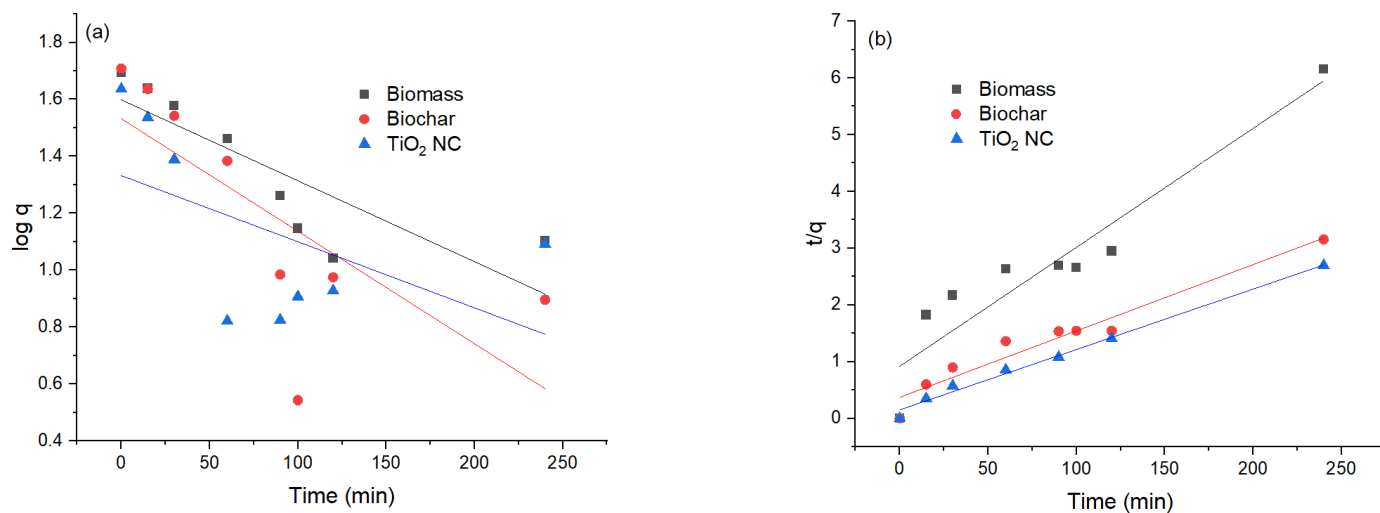


Figure 8. (a) Comparison of pseudo 1st-order graph; (b) pseudo 2nd-order graph.

### 3.4. Equilibrium Modeling

Adsorption isotherms of Cr(VI) from concentrations 10 to 100 ppm were studied with fixed pH 3, and an adsorbent dose of 0.1 g. Freundlich and Langmuir adsorption isotherms were used to define the relationship between adsorbent and adsorbate molecules in an aqueous solution. When there was a changing balance in adsorbate concentration in a large volume of solution with that of boundary, sorption equilibrium was established. To develop the equilibrium data, the primary concentration of Cr(VI) changed. The quantity of adsorbent was kept constant. To get the equilibrium data, the initial concentration of Cr(VI) was

changed whereas the number of biosorbents was kept constant. Contact time of 24 h was assured for equilibrium condition of sorption. The Freundlich and Langmuir adsorptions were on constant grade from the isotherm with a correlation coefficient for Cr(VI).

#### 3.4.1. Langmuir Isotherm

Generally, the Langmuir isotherm reveals that the surface of biosorbent and Cr(VI) has equal sites which have the same energy. According to this model, adsorbate molecules do not interact with each other but only interact with the site. Adsorption is restricted to monolayers. It is concluded that once a Cr(VI) ion adsorbs with a site, no more adsorption occurs. When equilibrium was achieved a monolayer appeared [43], which represents the plot of  $C_e/q_e$  (g/L) versus  $C_e$  (mg/L) under various concentrations of Cr(VI) sorption by MBM, BC and TiO<sub>2</sub> NC. Most of the points in this graph are out of linearity. The values obtained in the Freundlich model are greater than the R<sup>2</sup> value of the Langmuir model, which suggests the non-applicability of this model in interpreting sorption equilibrium data [44].

#### 3.4.2. Freundlich Isotherm

It presumes that monolayer adsorption distribution of active sites which are energetically heterogeneous, followed by interaction between biosorbents and adsorbed Cr(VI). The Freundlich isotherm equation is a mathematical expression that describes the adsorption of solute from an adsorbate solution to an adsorbent [44]. A graph is plotted of  $\log q_e$  versus  $\log C_e$ , this is either an indication that the intercept and graph slopes were used to calculate the value of  $1/n$  or that the adsorption stays continuous or is reduced by raising the concentration of adsorbents. Compared to the Langmuir isotherm plot, this showed more linearity. The value of R<sup>2</sup> is a result of the correlation coefficient near unity in the Freundlich model. The Freundlich and Langmuir adsorption constants were calculated from the isotherm with a correlation coefficient of Cr(VI). Cr(VI) was introduced to the Langmuir and Freundlich isotherm models. The Langmuir and Freundlich isotherms, however, were proven to be the finest suited and the equilibrium sorption information was well interpreted. A comparison of the values obtained from pseudo first-order and pseudo second-order is given in Table 4, and their graphical representation is in Figure 9a,b.

**Table 4.** Comparison of Langmuir and Freundlich models.

Adsorbate	Materials	Langmuir Model			Experimental Value		Freundlich Model		
		$X_m$ (mg/g)	KL (L/mg)	R <sup>2</sup>	Q q(mg/g)	q <sub>e</sub> (mg/g)	1/n	KF (mg/g)	R <sup>2</sup>
Chromium	Biomass	23.64	0.02	0.76	16.62	19.48	0.55	−2.14	0.98
	Biochar	26.45	0.08	0.72	19.97	31.94	0.57	−0.9	0.83
	TiO <sub>2</sub> Nc	59.17	0.04	0.85	42.36	47.22	0.61	−0.52	0.94

#### 3.5. Response Surface Methodology (RSM)

The main purpose of any designed experiment is to attain optimum response. RSM is one of the best techniques among all the available techniques. This process mainly helps to understand how test variables affect the selected process response, determine the possible interaction among the test variables, and characterize the combined effect of all test variables on the process response [45]. RSM is used to evaluate the effect of different parameters and for the prediction of targeted response to optimize the reaction. In the present research, interaction and optimization of three important independent variables, i.e., pH (A), initial concentration of Cr(VI) (B) and adsorbent dosage (C) were investigated by using Box–Behnken experimental design for the adsorption of Cr(VI) [46]. The main purpose of the developed model was to analyze the data of the experiment. The studentized residual and normal probability plot is depicted in Figure 10. It can be seen that there was neither any apparent problem with normality nor response transformation in Figure 10 [47].

All the dots lie near the regression line which showed a good correlation between the normal percentage probability and internally studentized residuals.

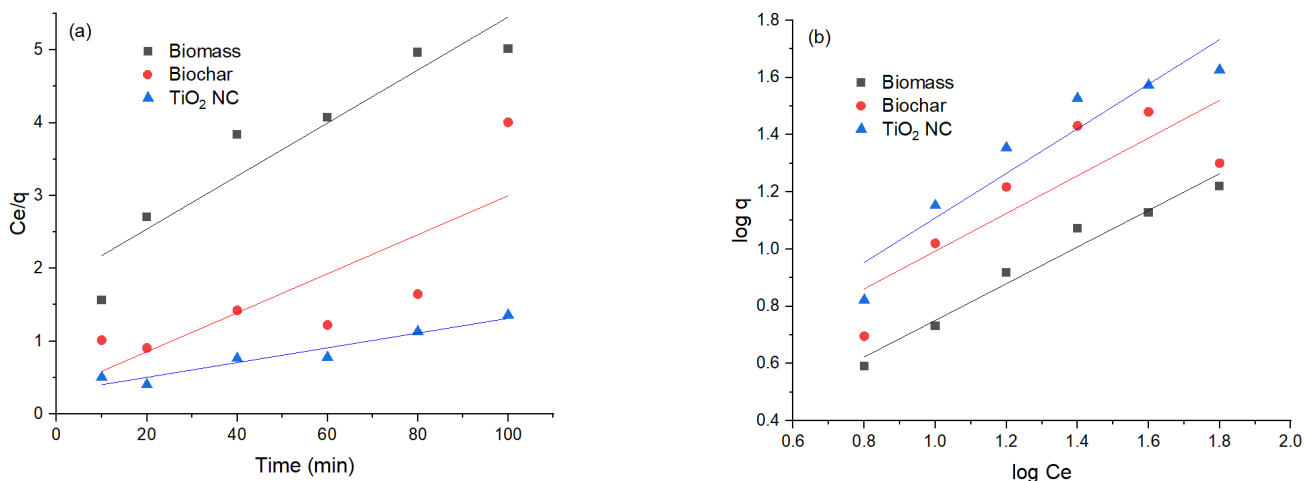


Figure 9. (a) Comparison of Langmuir isotherm; (b) Freundlich isotherm of lead adsorbed.

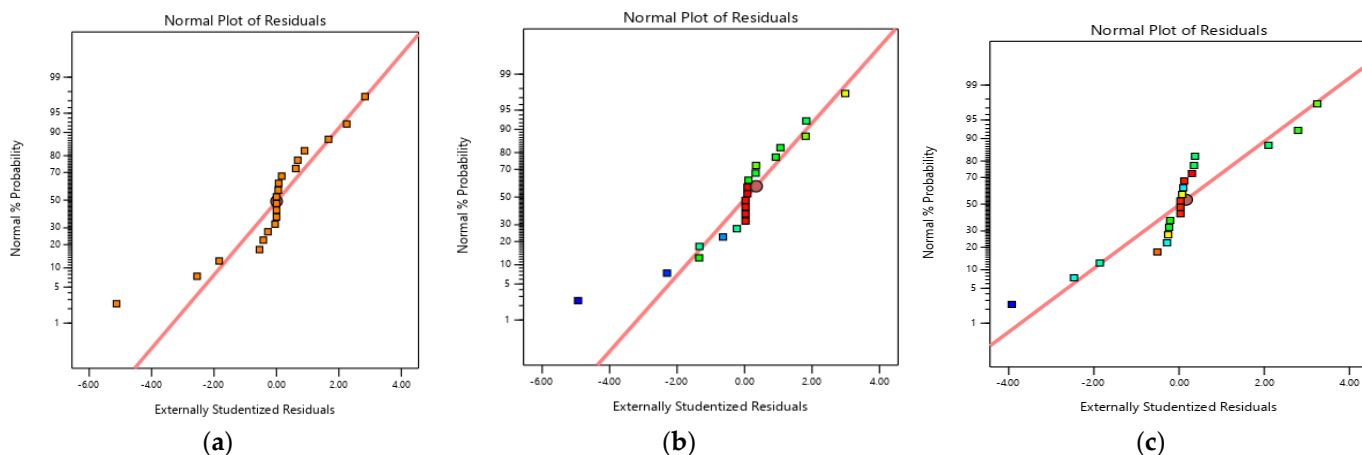


Figure 10. Studentized residuals and normal percentage probability plot for adsorption of Cr(VI) by (a) biomass; (b) biochar; and (c) TiO<sub>2</sub> NC.

### 3.5.1. Fitness of Quadratic Model

The values of coefficient of determination ( $R^2$ ) were checked to evaluate the fitness of the quadratic model for Cr(VI) adsorption.  $R^2$  measures the difference between model and predicted values from the mean value. The value of  $R^2$  should be close to 1.0 for a model with good prediction efficiency, However, the  $R^2$  value cannot be so reliable to assess the prediction efficiency of the model because the value of  $R^2$  is proportional to the number of terms in the model regardless of its statistical significance. So, a comparison of  $R^2$  with the value of adjusted  $R^2$  ( $R^2_{adj}$ ) values is a better way to assess prediction efficiency, as it reflects the number of factors in the experiment [48]. The value of  $R^2_{adj}$  often decreases if statistically insignificant variables are added. The large difference between the values of  $R^2$  and  $R^2_{adj}$  shows that some non-significant terms have been added to the model. A close correlation between predicted and experimental values can be indicated by the higher of the  $R^2$  and  $R^2_{adj}$  values. The obtained values of  $R^2$  and  $R^2_{adj}$  for MBM, BC and TiO<sub>2</sub> NC are given in Table 5.

**Table 5.**  $R^2$  and  $R^2_{adj}$  values of biomass, biochar and  $TiO_2$  NC.

Adsorbent	$R^2$	$R^2_{adj}$
Biomass	0.85	0.74
Biochar	0.91	0.82
$TiO_2$ NC	0.98	0.92

3.5.2. Effect of Independent Variables

The combined effect of pH and initial concentration on the adsorption of Cr(VI) was studied by varying the initial concentration from 10–100 ppm and pH range from 1–10, keeping the biosorbent dose constant at 0.1 g/100 mL Cr(VI) solution. The results are presented in a 3D plot in Figure 11. Solution pH greatly affects the Cr(VI) adsorption, as the solution chemistry of adsorbent and adsorbate is greatly affected by pH. Maximum removal was observed at a lower pH range [48].

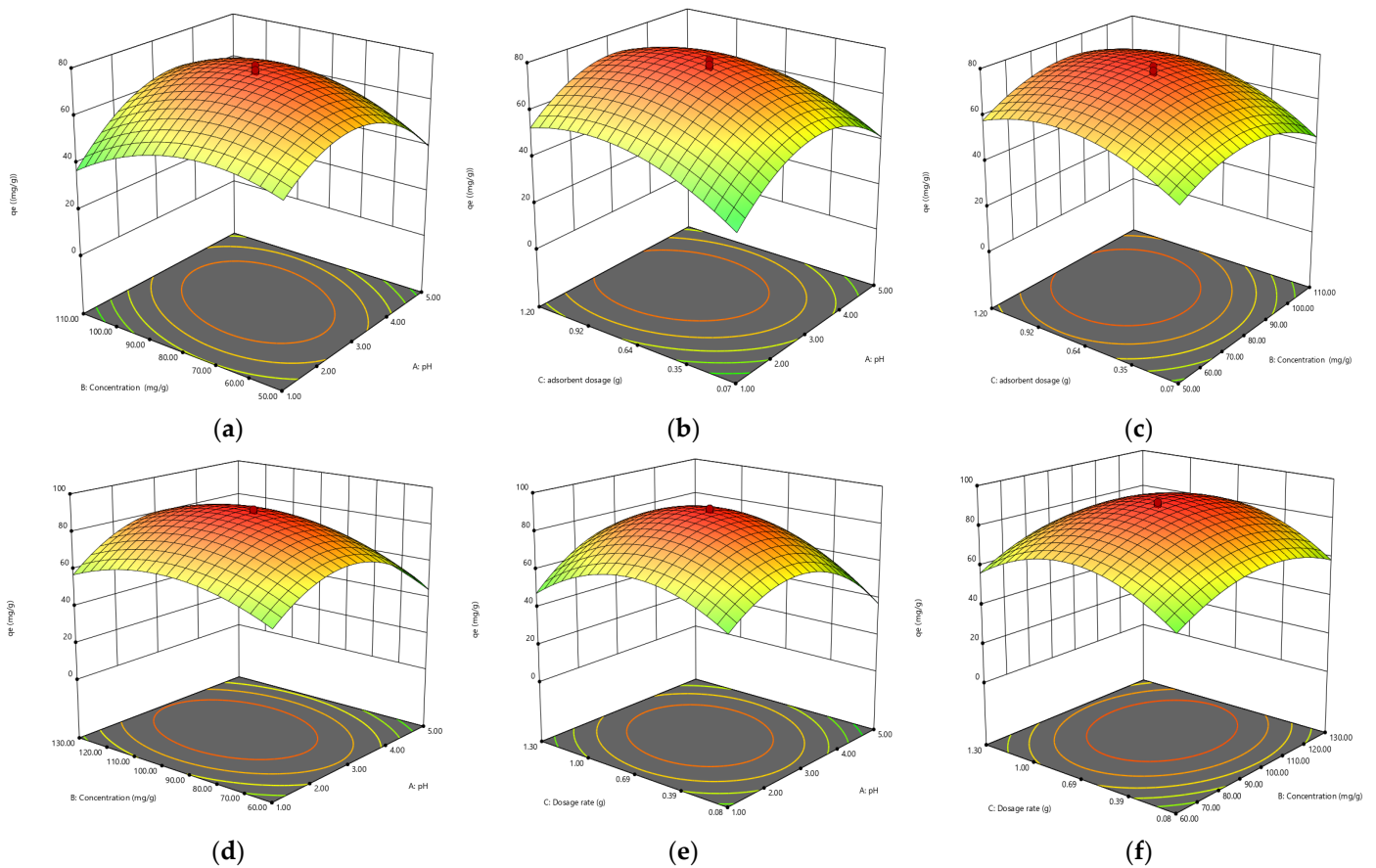


**Figure 11.** Cont.

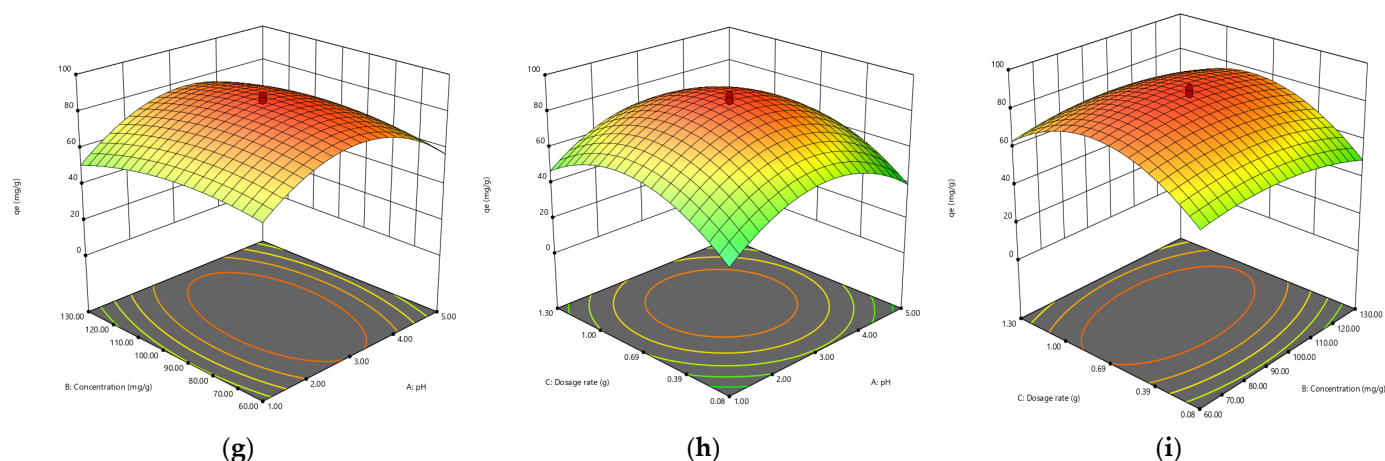


**Figure 11.** The 3D plots showing the interaction of (a) pH  $\times$  concentration, (b) pH  $\times$  adsorbent dosage, (c) concentration  $\times$  adsorbent dosage by biomass; (d) pH  $\times$  concentration, (e) pH  $\times$  adsorbent dosage, (f) concentration  $\times$  adsorbent dosage by biochar; (g) pH  $\times$  concentration, (h) pH  $\times$  adsorbent dosage, (i) concentration  $\times$  adsorbent dosage by TiO<sub>2</sub> NC for adsorption of Cr(VI).

The combined effect of adsorbent dosage and pH Cr(VI) adsorption was studied by varying the adsorbent dosage from 0.05–0.10 ppm and pH from 1–10, keeping the initial concentration constant. The process of biosorption is significantly affected by the dosage of adsorption. The adsorption capacity (mg/g) of biosorbent decreases with the increase in biosorbent dosage from 0.05 to 0.1 g/100 ppm Cr(VI) solution. It might be due to aggregation or overlapping of active sites, which results in an increase in diffusion path length and a decrease in total surface area available for biosorption of Cr(VI). The highest removal was obtained by using increasing amounts of biosorbents. The results are presented in a 3D plot in Figure 11.

The combined effect of initial concentration solution and biosorbent dose on the Cr(VI) adsorption was studied by varying the biosorbent dosage from 0.05 to 0.1 g and initial adsorbate concentration from 10 to 100 mg/L, keeping the pH adjusted to 3. The results are presented in Figure 11. The biosorption process is strongly controlled by initial concentration. The mass transfer resistance between the aqueous and solid phases is controlled by it. The biosorption of Cr(VI) is affected by both the independent variables. Figure 11 is indicating that the amount of Cr(VI) adsorbed per unit mass of biosorbent is proportional to an increase in the initial concentration of Cr(VI) solution from 10 to 100 mg/L. Maximum removal of Cr(VI) (mg/g) was seen at higher initial concentrations, the reason for this could be the decrease in resistance to uptake the adsorbate from Cr(VI) solution at higher initial concentrations.

#### 4. Conclusions

The present research work compared the adsorption efficiency of MBM, BC and biochar-based TiO<sub>2</sub> NC for Cr(VI). Among these, the synthesized novel nanocomposite has been proven very effective for the removal of heavy metals. In the present research work, potato peel and banana peel were ground to make biomass. Prepared biomass (MBM) was then pyrolyzed to make biochar (BC). Leaves of *Psidium guajava* were utilized to prepare TiO<sub>2</sub> NP by using titanium precursors. Then prepared biochar was sonicated with TiO<sub>2</sub> NP to make nanocomposite for better adsorption of heavy metals. Several parameters such as initial concentration of heavy metals, pH, contact time and dosage rate were optimized. The percentage removal of Cr(VI) was investigated, maximum adsorption of Cr(VI) was at pH 3, decrease when the concentration is increased, while percentage removal increases as dosage rate are increased and contact time. The uptake capacity of heavy metals from aqueous solution was in the order biomass (78 mg/L) < biochar (89 mg/L) < TiO<sub>2</sub> NC (90 mg/L), among them, NC was confirmed with maximum uptake capacity. The Langmuir model

better explained the adsorption process of heavy metals as compared to the Freundlich model. Response surface methodology (RSM) was utilized for the optimization of each operational variable.

**Author Contributions:** Data curation, A.A., R.N., S.N. and Z.A.; Formal analysis, A.A., R.N., H.G., U.R., S.N., N.A. and M.Z.A.; Investigation, R.N., U.R., M.A., Fahad A. Alharthi and E.A.K.; Methodology, A.A., R.N., U.R., S.N., S.u.R., Z.A., M.A., N.A. and M.Z.A.; Project administration, U.R. and F.A.A.; Resources, R.N., H.G., U.R., S.u.R., F.A.A. and E.A.K.; Supervision, R.N.; Visualization, U.R.; Writing—original draft, R.N., S.u.R., M.A. and N.A.; Writing—review & editing, H.G., U.R., F.A.A. and E.A.K. All authors have read and agreed to the published version of the manuscript.

**Funding:** Authors extend their thanks to Researchers Supporting Project (RSP-2021/160), King Saud University, Riyadh, Saudi Arabia.

**Institutional Review Board Statement:** Not applicable.

**Informed Consent Statement:** Not applicable.

**Data Availability Statement:** Not applicable.

**Conflicts of Interest:** The authors declare no conflict of interest.

## References

1. Siddiqui, S.I.; Fatima, B.; Tara, N.; Rathi, G.; Chaudhry, S.A. Recent advances in remediation of synthetic dyes from wastewaters using sustainable and low-cost adsorbents. In *The Impact and Prospects of Green Chemistry for Textile Technology*; Shahid-ul-Islam, Butola, B.S., Eds.; Woodhead Publishing: Sawston, UK, 2019; pp. 471–507.
2. Vu, C.T.; Lin, C.; Shern, C.-C.; Yeh, G.; Tran, H.T. Contamination, ecological risk and source apportionment of heavy metals in sediments and water of a contaminated river in Taiwan. *Ecol. Indic.* **2017**, *82*, 32–42. [[CrossRef](#)]
3. Ognibene, G.; Gangemi, C.; Spitaleri, L.; Gulino, A.; Purrello, R.; Cicala, G.; Fragalà, M.E. Role of the surface composition of the polyethersulfone–TiP–H2T4 fibers on lead removal: From electrostatic to coordinative binding. *J. Mater. Sci.* **2019**, *54*, 8023–8033. [[CrossRef](#)]
4. Anderson, A.; Anbarasu, A.; Pasupuleti, R.R.; Sekar, M.; Praveenkumar, T.R.; Kumar, J.A. Treatment of heavy metals containing wastewater using biodegradable adsorbents: A review of mechanism and future trends. *Chemosphere* **2022**, *295*, 133724. [[CrossRef](#)] [[PubMed](#)]
5. Janani, R.; Gurunathan, B.; Sivakumar, K.; Varjani, S.; Ngo, H.H.; Gnansounou, E. Advancements in heavy metals removal from effluents employing nano-adsorbents: Way towards cleaner production. *Environ. Res.* **2022**, *203*, 111815.
6. Burakov, A.E.; Galunin, E.V.; Burakova, I.V.; Kucherova, A.E.; Agarwal, S.; Tkachev, A.G.; Gupta, V.K. Adsorption of heavy metals on conventional and nanostructured materials for wastewater treatment purposes: A review. *Ecotoxicol. Environ. Saf.* **2018**, *148*, 702–712. [[CrossRef](#)]
7. Fiorenza, R.; Di Mauro, A.; Cantarella, M.; Iaria, C.; Scalisi, E.M.; Brundo, M.V.; Gulino, A.; Spitaleri, L.; Nicotra, G.; Dattilo, S.; et al. Preferential removal of pesticides from water by molecular imprinting on TiO<sub>2</sub> photocatalysts. *Chem. Eng. J.* **2020**, *379*, 122309. [[CrossRef](#)]
8. Tatarchuk, T.; Bououdina, M.; Al-Najar, B.; Bitra, R.B. Green and ecofriendly materials for the remediation of inorganic and organic pollutants in water. A new generation material graphene. In *Applications in Water Technology*; Springer: Berlin/Heidelberg, Germany, 2019; pp. 69–110.
9. Gulino, A.; Papanikolaou, G.; Lanzafame, P.; Aaliti, A.; Primerano, P.; Spitaleri, L.; Lo Schiavo, S. Synthesis, characterization and photocatalytic behavior of SiO<sub>2</sub>@ nitrized-TiO<sub>2</sub> nanocomposites obtained by a straightforward novel approach. *Chem. Open* **2021**, *10*, 1033–1040.
10. Kumari, P.; Alam, M.; Siddiqi, W.A. Usage of nanoparticles as adsorbents for wastewater treatment: An emerging trend. *Sustain. Mater. Technol.* **2019**, *22*, e00128.
11. Fiorenza, R.; Bellardita, M.; Balsamo, S.A.; Spitaleri, L.; Gulino, A.; Condorelli, M.; Palmisano, L. A solar photothermocatalytic approach for the CO<sub>2</sub> conversion: Investigation of different synergisms on CoO-CuO/brookite TiO<sub>2</sub>-CeO<sub>2</sub> catalysts. *Chem. Eng. J.* **2022**, *428*, 131249. [[CrossRef](#)]
12. Chen, D.; Cheng, Y.; Zhou, N.; Chen, P.; Wang, Y.; Li, K.; Ruan, R. Photocatalytic degradation of organic pollutants using TiO<sub>2</sub>-based photocatalysts: A review. *J. Clean. Prod.* **2020**, *268*, 121725. [[CrossRef](#)]
13. Zimbone, M.; Cacciato, G.; Spitaleri, L.; Egdell, R.G.; Grimaldi, M.G.; Gulino, A. Sb-doped titanium oxide: A rationale for its photocatalytic activity for environmental remediation. *ACS Omega* **2018**, *3*, 11270–11277. [[CrossRef](#)] [[PubMed](#)]
14. El-Azazy, M.; El-Shafie, A.S.; Issa, A.A.; Al-Sulaiti, M.; Al-Yafie, J.; Shomar, B.; Al-Saad, K. Potato peels as an adsorbent for heavy metals from aqueous solutions: Eco-structuring of a green adsorbent operating Plackett–Burman design. *J. Chem.* **2019**, *1*, 4926240. [[CrossRef](#)]

15. Ali, A. Removal of Mn (II) from water using chemically modified banana peels as efficient adsorbent. *Environ. Nanotechnol. Monit. Manag.* **2017**, *7*, 57–63. [[CrossRef](#)]
16. Arifiyana, D.; Devianti, V.A. Optimization of pH and contact time adsorption of banana peels as adsorbent of Co(II) and Ni(II) from liquid solutions. *AIP Conf. Proceed.* **2021**, *2330*, 070007.
17. Sahoo, J.K.; Hota, A.; Khuntia, A.K.; Sahu, S.; Sahoo, S.K.; Sabar, A.K.; Rath, J. Removal of dyes using various organic peel-based materials: A systematic review. *Appl. NanoBioSci.* **2022**, *11*, 3714–3727.
18. Regkouzias, P.; Diamadopoulou, E. Adsorption of selected organic micro-pollutants on sewage sludge biochar. *Chemosphere* **2019**, *224*, 840–851. [[CrossRef](#)]
19. Zhou, N.; Chen, H.; Xi, J.; Yao, D.; Zhou, Z.; Tian, Y.; Lu, X. Biochars with excellent Pb (II) adsorption property produced from fresh and dehydrated banana peels via hydrothermal carbonization. *Bioresour. Technol.* **2017**, *232*, 204–210. [[CrossRef](#)]
20. Youssef, A.M.; El-Sayed, S.M. Bionanocomposites materials for food packaging applications: Concepts and future outlook. *Carbohydr. Polym.* **2018**, *193*, 19–27. [[CrossRef](#)]
21. Rehman, R.; Farooq, S.; Mahmud, T. Use of agro-waste *Musa acuminata* and *Solanum tuberosum* peels for economical sorptive removal of emerald green dye in ecofriendly way. *J. Clean. Prod.* **2019**, *206*, 819–826. [[CrossRef](#)]
22. Sakthivel, T.; Ramachandran, R.; Kirubakaran, K. Photocatalytic properties of copper-two-dimensional graphitic carbon nitride hybrid film synthesized by pyrolysis method. *J. Environ. Chem. Eng.* **2018**, *6*, 2636–2642. [[CrossRef](#)]
23. Deshmukh, K.K.; Hase, G.J.; Gaje, T.R.; Phatangare, N.D.; Shilpa, G.; Ashwini, V. Titanium oxide nanoparticles and degradation of dye by nanoparticles. *Int. J. Mater. Sci.* **2018**, *13*, 23–30.
24. Sunderishwary, S.; Kaus, N.H.M.M.; Jiang, Z.-T.; Altarawneh, M.; Lee, H.L. Green synthesis of mesoporous anatase TiO<sub>2</sub> nanoparticles and their photocatalytic activities. *RSC Adv.* **2017**, *7*, 48083–48094.
25. Dey, A.; Nangare, V.; More, P.V.; Khan, M.A.S.; Khanna, P.K.; Sikder, A.K.; Chattopadhyay, S. A graphene titanium dioxide nanocomposite (GTNC): One pot green synthesis and its application in a solid rocket propellant. *RSC Adv.* **2015**, *5*, 63777–63785. [[CrossRef](#)]
26. Ayawei, N.; Ebelegi, A.N.; Wankasi, D. Modelling and interpretation of adsorption isotherms. *J. Chem.* **2017**, *2017*, 3039817. [[CrossRef](#)]
27. Bian, H.; Wan, J.; Muhammad, T.; Wang, G.; Sang, L.; Jiang, L.; Lou, Z. Computational study and optimization experiment of nZVI modified by anionic and cationic polymer for Cr (VI) stabilization in soil: Kinetics and response surface methodology (RSM). *Environ. Pollut.* **2021**, *276*, 116745. [[CrossRef](#)]
28. Liang, S.; Han, Y.; Wei, L.; McDonald, A.G. Production and characterization of bio-oil and bio-char from pyrolysis of potato peel wastes. *Biomass Convers. Biorefinery* **2015**, *5*, 237–246. [[CrossRef](#)]
29. Subhapriya, S.; Gomathipriya, P. Green synthesis of titanium dioxide (TiO<sub>2</sub>) nanoparticles by *Trigonella foenum-graecum* extract and its antimicrobial properties. *Microb. Pathog.* **2018**, *116*, 215–220. [[CrossRef](#)]
30. Dutta, A. Fourier transform infrared spectroscopy. In *Spectroscopic Methods for Nanomaterials Characterization*; Thomas, S., Thomas, R., Zachariah, A.K., Mishra, R.K., Eds.; Elsevier: Amsterdam, The Netherlands, 2017; pp. 73–93.
31. Thamaphat, K.; Limsuwan, P.; Ngotawornchai, B. Phase characterization of TiO<sub>2</sub> powder by XRD and TEM. *Agric. Nat. Resour.* **2008**, *42*, 357–361.
32. Ijadpanah-Saravy, H.; Safari, M.; Khodadadi-Darban, A.; Rezaei, A. Synthesis of titanium dioxide nanoparticles for photocatalytic degradation of cyanide in wastewater. *Anal. Lett.* **2014**, *47*, 1772–1782. [[CrossRef](#)]
33. Khairiah, K.; Frida, E.; Sebayang, K.; Sinuhaji, P.; Humaidi, S. Data on characterization, model, and adsorption rate of banana peel activated carbon (*Musa acuminata*) of various heavy metals (Mn, Pb, Zn, Fe). *Data Brief* **2021**, *39*, 107611. [[CrossRef](#)]
34. Hasanin, M.S. Simple, economic, ecofriendly method to extract starch nanoparticles from potato peel waste for biological applications. *Starch-Stärke* **2021**, *73*, 2100055. [[CrossRef](#)]
35. Selvarajoo, A.; Muhammad, D.; Arumugasamy, S.K. An experimental and modelling approach to produce biochar from banana peels through pyrolysis as potential renewable energy resources. *Modeling Earth Syst. Environ.* **2020**, *6*, 115–128. [[CrossRef](#)]
36. Touihri, M.; Guesmi, F.; Hannachi, C.; Hamrouni, B.; Sellaoui, L.; Badawi, M.; Fiol, N. Single and simultaneous adsorption of Cr (VI) and Cu (II) on a novel Fe<sub>3</sub>O<sub>4</sub>/pine cones gel beads nanocomposite: Experiments, characterization and isotherms modeling. *Chem. Eng. J.* **2021**, *416*, 129101. [[CrossRef](#)]
37. Chen, H.; Zhang, Z.; Zhong, X.; Zhuo, Z.; Tian, S.; Fu, S.; Liu, Y. Constructing MoS<sub>2</sub>/Lignin-derived carbon nanocomposites for highly efficient removal of Cr (VI) from aqueous environment. *J. Hazard. Mater.* **2021**, *408*, 124847. [[CrossRef](#)]
38. Maheswari, B.U.; Sivakumar, V.M.; Thirumarimurugan, M. Sequester adsorption of Cr (VI) and Pb (II) ions from aqueous solution by green synthesized nanocomposite (OB/ZnO): Characterization, kinetics, isotherm and mechanism. *Environ. Nanotechnol. Monit. Manag.* **2022**, *18*, 100680. [[CrossRef](#)]
39. Sarojini, G.; Babu, S.V.; Rajamohan, N.; Kumar, P.S.; Rajasimman, M. Surface modified polymer-magnetic-algae nanocomposite for the removal of chromium-equilibrium and mechanism studies. *Environ. Res.* **2021**, *201*, 111626. [[CrossRef](#)]
40. Samuel, M.S.; Bhattacharya, J.; Raj, S.; Santhanam, N.; Singh, H.; Pradeep Singh, N.D. Efficient removal of Chromium (VI) from aqueous solution using chitosan grafted graphene oxide (CS-GO) nanocomposite. *Int. J. Biol. Macromol.* **2019**, *121*, 285–292. [[CrossRef](#)]
41. Ho, Y.; McKay, G.; Hong, T.; Bay, W.; Kong, H.; Hong, T. Kinetics of pollutant sorption by biosorbents: Review. *Sep. Purif. Rev.* **2000**, *29*, 189–232. [[CrossRef](#)]

42. Sari, A.; Tuzen, M.; Citak, D.; Soylak, M. Equilibrium, kinetic and thermodynamic studies of adsorption of Pb (II) from aqueous solution onto Turkish kaolinite clay. *J. Hazard. Mater.* **2007**, *149*, 283–291. [[CrossRef](#)]
43. Huang, Y.-T.; Shih, M.-C. Effect of linearized expressions of Langmuir equations on the prediction of the adsorption of methylene blue on rice husk. *Source Int. J. Sci. Res. Publ.* **2016**, *6*, 549–554.
44. Chung, H.-K.; Kim, W.-H.; Park, J.; Cho, J.; Jeong, T.-Y.; Park, P.-K. Application of Langmuir and Freundlich isotherms to predict adsorbate removal efficiency or required amount of adsorbent. *J. Ind. Eng. Chem.* **2015**, *28*, 241–246. [[CrossRef](#)]
45. Özer, A.; Gürbüz, G.; Çalimli, A.; Körbahti, B.K. Biosorption of copper (II) ions on *Enteromorpha prolifera*: Application of response surface methodology (RSM). *Chem. Eng. J.* **2009**, *146*, 377–387. [[CrossRef](#)]
46. Pillai, M.G.; Regupathi, I.; Kalavathy, M.H.; Murugesan, T.; Miranda, L.R. Optimization and analysis of nickel adsorption on microwave irradiated rice husk using response surface methodology (RSM). *J. Chem. Technol. Biotechnol.* **2009**, *84*, 291–301. [[CrossRef](#)]
47. Yi, S.; Su, Y.; Qi, B.; Su, Z.; Wan, Y. Application of response surface methodology and central composite rotatable design in optimizing the preparation conditions of vinyltriethoxysilane modified silicalite/polydimethylsiloxane hybrid pervaporation membranes. *Sep. Purif. Technol.* **2010**, *71*, 252–262. [[CrossRef](#)]
48. Lucas, J.M. Response surface methodology. In *Process and Product Optimization Using Designed Experiments*; Taylor & Francis: Abingdon, UK, 2010.